Inorganic Chemistry

Article

pubs.acs.org/IC

Magnetic Properties and Electronic Structure of Manganese-Based Blue Pigments: A High-Frequency and -Field EPR Study

J. Krzystek,*[,§] Joshua Telser,[¶] Jun Li,[†] and M. A. Subramanian*[,†]

[§]National High Magnetic Field Laboratory, Florida State University, Tallahassee, Florida 32310, United States

[¶]Department of Biological, Chemical, and Physical Sciences, Roosevelt University, Chicago, Illinois 60605, United States

[†]Department of Chemistry, Oregon State University, Corvallis, Oregon 97331, United States

Supporting Information

ABSTRACT: A variety of new oxide-based materials based on hexagonal phase of $YInO_3$ have been recently described. In some of these materials, the In(III) ions are substituted by Mn(III), which finds itself in a trigonal-bipyramidal (TBP) coordination environment. While $YInO_3$ is colorless and $YMnO_3$ is black, mixed systems $YIn_{1-x}Mn_xO_3$ ($0.02 < x < 0.25$) display intense blue color and have been proposed as novel blue pigments. Since the Mn(III) ion is paramagnetic, its presence imparts distinct magnetic properties to the whole class of materials. These properties were investigated by electron paramagnetic resonance (EPR) in its high-frequency and -field version (HFEPR), a technique ideally suited for transition metal ions such as Mn(III) that, in contrast to, for example, Mn(II), are difficult to study by EPR at (conventional) low frequency and field. $YIn_{1-x}Mn_xO_3$ with $0.02 < x < 0.2$ exhibited high-quality HFEPR spectra up to room temperature that could be interpreted as arising from isolated $S = 2$ paramagnets. A simple ligand-field model, based on the structure and optical spectra, explains the spin Hamiltonian parameters provided by HFEPR, which were $D = +3.0\ cm^{-1}$, $E = 0$; $g_\perp = 1.99$, $g_\parallel = 2.0$. This study demonstrates the general applicability of a combined spectroscopic and classical theoretical approach to understanding the electronic structure of novel materials containing paramagnetic dopants. Moreover, HFEPR complements optical and other experimental methods as being a sensitive probe of dopant level.

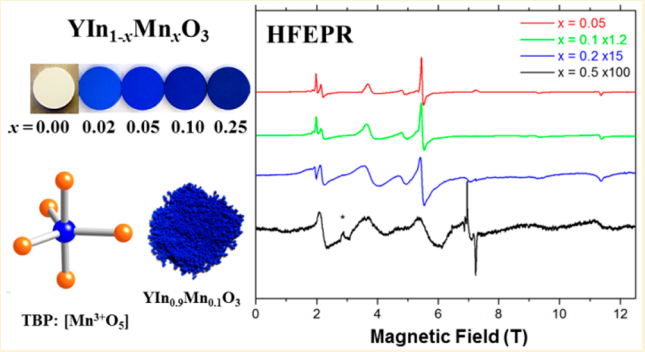

INTRODUCTION

Some of us have recently prepared and reported on a class of compounds that can be described as solid solutions of the oxides of a general formula $YIn_{1-x}Mn_xO_3$, where $0 < x < 1$.[1] The common characteristic of the two extreme cases of this series, that is, $YInO_3$ and $YMnO_3$, is that both can be prepared in hexagonal crystal structures, which result in the metal ion (In(III) or Mn(III)) finding itself on a site with trigonal symmetry, in a pentacoordinate, trigonal bipyramidal (TBP) oxygen donor coordination (Figure 1). The most interesting finding was that this type of environment for Mn(III) affects the optical properties of the solid solution. While pure $YInO_3$ is colorless, and $YMnO_3$ is black, the mixed systems display a vivid blue color for a wide range of $0.02 < x < 0.25$ due to a new band in the electronic absorption spectrum with a maximum at ~2 eV (16 100 cm^{-1}, 620 nm). The appearance of this band was attributed to a Laporte allowed (*xy* polarization) excitation of an electron from the $d_{xy},d_{x^2-y^2}$ orbital (e' representation in D_{3h} symmetry) of Mn(III) to its highest-lying orbital (d_{z^2}; a_1'), which lies within an energy gap of $YInO_3$ (Figure 1).[1] The higher-energy transition, which is from the lowest-energy Mn(III) orbitals d_{xy},d_{yz} (e'') to d_{z^2}, is forbidden in D_{3h} symmetry, although it is allowed in C_{3v} symmetry. Because of this optical property, which has been confirmed in a variety of other mixed-ion systems, compounds of the type described here have been proposed as novel blue pigments for industrial applications.[2]

Since Mn(III) is a paramagnetic ion, the properties of its oxides have also become an object of magnetic investigations.[4] Pure $YMnO_3$ is known for its multiferroic properties with a Néel temperature of paramagnetic/ferromagnetic transition equal to ~75 K.[5] Magnetic studies of the $YIn_{1-x}Mn_xO_3$ mixed systems where Mn(III) is in the high-spin (HS) form ($3d^4$, $S = 2$) revealed that this temperature decreases upon lowering the coefficient *x*, and the transition is completely suppressed for $x < 0.5$. The magnetic properties of $YIn_{1-x}Mn_xO_3$ systems have been of continued interest, and in this work we concentrate on the single-ion properties of HS Mn(III) in what is an unusual coordination environment. As a measurement technique we used electron paramagnetic resonance (EPR). Since HS Mn(III) coordination complexes typically display a considerable zero-field splitting (zfs), we used EPR in high-frequency and -field conditions, known as HFEPR.[6] Previous HFEPR studies of Mn(III) complexes were concentrated on either

Received: June 11, 2015
Published: September 4, 2015

DOI: 10.1021/acs.inorgchem.5b01306
Inorg. Chem. 2015, 54, 9040−9045

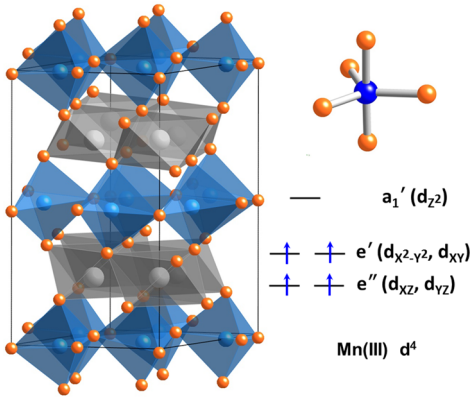

Figure 1. (left) Structure of $YMnO_3$ showing layers of MnO_5 trigonal bipyramids (TBP) in blue interspersed with layers of YO_6 octahedra (Y, gray spheres). (upper right) Detailed view (Mn, blue spheres; O, orange spheres). (lower right) Schematic energy levels for the spin-up Mn(III) 3d orbitals in TBP coordination are shown. With use of the AOM including only σ-bonding, the energy of the e'' orbitals is zero, the e' orbitals are at $(9/8)\varepsilon_\sigma$, and the a_1' orbital is at $(22/8)\varepsilon_\sigma$. If π-bonding is included, then the energies are as follows: $(7/2)\varepsilon_\pi(e'')$; $(9/8)\varepsilon_\sigma + (3/2)\varepsilon_\pi$ (e'); $(22/8)\varepsilon_\sigma(a_1')$.[3]

square-pyramidal coordination as found, for example, in porphyrinoid complexes[7−10] or in more or less distorted octahedral coordination as found in many other complexes,[11−23] including a very early study on a Mn^{3+}-doped oxide (rutile).[24] An interesting HS Mn(III) coordination complex with distorted TBP geometry ($N3_{eq}(N,O)_{ax}$ donor set) has been recently reported and studied by conventional EPR,[25] but HFEPR was not used, despite its potential suitability. Systems with $S = 2$, most commonly Fe(II) and Mn(III), can exhibit X-band EPR spectra at low fields (high effective g values) due to rhombic splitting of the $|S, M_S\rangle = |2, \pm 2\rangle$ state,[25−29] but extraction of a unique set of spin Hamiltonian parameters from those spectra is not guaranteed, as shown, for example, in $Mn(acac)_3$.[15]

EXPERIMENTAL SECTION

Samples were prepared as described previously.[1] HFEPR data were acquired using either of two facilities located at the NHMFL. The Electron Magnetic Resonance (EMR) Facility includes a spectrometer described elsewhere,[30] modified by the use of Virginia Diodes Inc. (VDI, Charlottesville, VA) sources, operating in a 50−420 GHz frequency range. The spectrometer is associated with a 17 T superconducting magnet. The DC Facility includes a setup using tunable sources (backward wave oscillators (BWOs)), routinely operating in a 100−700 GHz frequency range and is associated with the 25 T resistive Bitter-type "Keck" magnet.[31] In both cases an InSb bolometer (QMC, Cardiff, Wales) is used as a detector. The necessary modulation was obtained either through modulating the magnetic field ("magnetic modulation") or chopping the sub-THz wave beam ("optical modulation"). In both cases the signal was converted from alternating current to direct current by a lock-in amplifier (Stanford SR-830). The samples of the Mn(III) concentration coefficients, x = 0.05, 0.1, 0.2, and 0.5, were used "as is" in a powder form. Approximately 100−200 mg of material was employed in each case.

RESULTS AND DISCUSSION

All samples showed strong and well-defined EPR responses over the complete frequency region, and in a wide temperature range from liquid helium to ambient. Figure 2 shows HFEPR spectra of the four samples differing by the concentration of Mn(III) at a fixed frequency (203.2 GHz) and temperature (10 K).

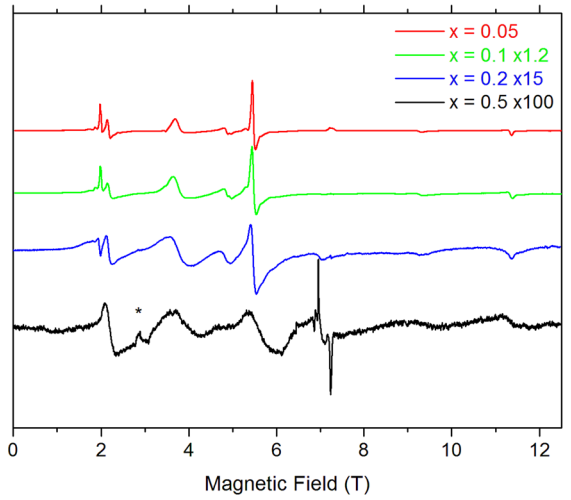

Figure 2. Representative HFEPR spectra of $YIn_{1-x}Mn_xO_3$ samples differing by the Mn(III) content (x) recorded at 203.2 GHz and 10 K. The spectra were obtained using magnetic modulation resulting in a derivative shape. The amplitudes are approximately normalized. The narrow resonances near $g = 2$ (7 T), visible particularly well in the x = 0.5 sample due to the large magnification factor, originate from $g \approx 2$ impurities. The feature near 3 T marked with an asterisk is caused by solid molecular dioxygen. Neither is simulated.

The resonances clearly originate from an $S > 1/2$ state and bear a strong similarity to those of known Mn(III) EPR powder spectra. Upon visual inspection, their linewidth increases with increasing Mn(III) content under the given conditions.[32] A more detailed linewidth analysis was postponed until spin Hamiltonian parameters could first be determined for the Mn(III) ion. For this purpose we followed the tunable-frequency EPR procedure, which depends on collecting turning points in the powder spectra, and fitting the parameters to the complete two-dimensional (field vs frequency) array.[33] Figure 3 shows such a field/frequency map of turning points collected for the sample $YIn_{0.95}Mn_{0.05}O_3$ at 4.2−10 K.

The field/frequency map shown in Figure 3 is characteristic for an $S = 2$ spin state and axial zfs tensor with the zero-field transitions occurring at ∼90, 270, and 360 GHz, corresponding to the approximate values of $|D|$, $3|D|$, and $4|D|$, respectively (for the energy diagram explaining these transitions, see Figure S1 in the Supporting Information). The precise values of the spin Hamiltonian parameters were obtained by a proper computer least-squares fit and are listed in Table 1. We performed the same procedure for samples with x = 0.05, 0.1, and x = 0.2, but not for the one with x = 0.5 due to excessive linewidths and the correspondingly large error in determining the exact position of the resonances (the parameters for x = 0.5 given in Table 1 are thus estimates). The corresponding field/frequency maps for x = 0.1 and x = 0.2 are shown in Figures S2 and S3, respectively, in the Supporting Information. We did not observe a significant dependence of D on the temperature in the diluted systems; however, we saw a "collapse" of the zfs into one averaged signal in the x = 0.5 sample at high temperatures (vide supra).

To ascertain the sign of D we simulated single-frequency powder spectra. Figure 4 shows a spectrum of $YIn_{0.9}Mn_{0.1}O_3$ at 4.2 K and 260 GHz, obtained with a BWO using an optical

DOI: 10.1021/acs.inorgchem.5b01306
Inorg. Chem. 2015, 54, 9040−9045

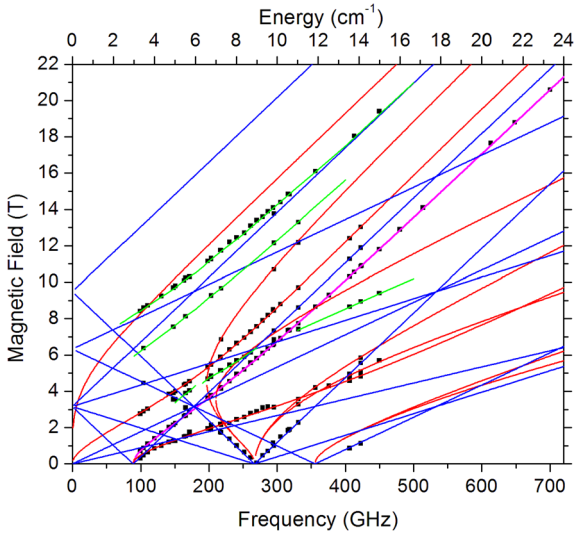

Figure 3. Field/frequency map of resonances in $YIn_{0.95}Mn_{0.05}O_3$ at 4.2−10 K. The squares are experimental turning points, while the lines were drawn using best-fitted spin Hamiltonian parameters listed in Table 1. Red lines: magnetic field perpendicular to the z axis of the zfs tensor; blue lines: field parallel; green lines: off-axis turning points. The perpendicular turning point of the $|2, -1\rangle \rightarrow |2, 0\rangle$ transition that was used for line width comparison (Table 2) is mapped with a thicker magenta line.

Table 1. Spin Hamiltonian Parameters of the Mn(III) Ion in Trigonal Bipyramidal Configuration As Found in the $YIn_{1-x}Mn_xO_3$ Solid Solutions at Low Temperatures

sample	D (cm^{-1})	E (cm^{-1})	$g_\perp$	$g_\parallel$
$YIn_{0.95}Mn_{0.05}O_3$	+2.965(3)	0.006(1)	1.987(2)	2.008(5)
$YIn_{0.9}Mn_{0.1}O_3$	+2.957(7)	0.003(3)	1.987(3)	2.005(7)
$YIn_{0.8}Mn_{0.2}O_3$	+2.97(1)	0.015(5)	1.987(4)	1.988(6)
$YIn_{0.5}Mn_{0.5}O_3$	ca. +3	∼0	∼2.00	∼2.00

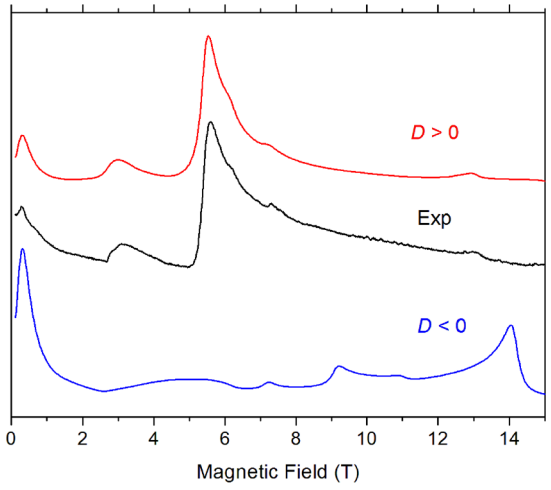

Figure 4. An HFEPR spectrum of $YIn_{0.9}Mn_{0.1}O_3$ at 4.2 K and 260 GHz (black trace), which is close to the zero-field resonance at 270 GHz. The spectrum was obtained with a BWO source, in a resistive magnet, and using optical modulation resulting in an absorptive spectral shape (instead of derivative shape such as that in Figure 2). The colored traces are simulations: the red trace using a positive and the blue one a negative value of D, with $|D| = 2.96$ cm^{-1}, $E = 0$, and $g_{iso} = 2.00$. The single-crystal line width used in the simulations was 100 mT.

modulation resulting in an absorptive spectral shape, together with two simulations: one using a negative and the other a positive value of D. A visual comparison of the experimental spectrum with the simulated ones clearly shows that D for $x = 0.1$ (and all other values of x investigated) is positive. Similar plots corresponding to different frequencies, one lower, 109 GHz, and one higher, 406 GHz, are shown in Figures S4 and S5, respectively, in the Supporting Information.

As briefly mentioned above, the EPR linewidth strongly depends on the Mn(III) content in the solid solution. The approximate values are collected in Table 2 for one particular

Table 2. Observed Line Width ΔB_{pp} of the $|S, M_S\rangle = |2, -1\rangle \rightarrow |2, 0\rangle$ Transition at 10 K and 203 GHz, Occurring at ∼5.45 T in Figure 2, as a Function of Mn Doping Level (x = 0.05, 0.1, 0.2, 0.5)

sample	ΔB_{pp} (mT)[a]
$YIn_{0.95}Mn_{0.05}O_3$	70
$YIn_{0.9}Mn_{0.1}O_3$	100
$YIn_{0.8}Mn_{0.2}O_3$	140
$YIn_{0.5}Mn_{0.5}O_3$	710

[a]The same turning point is seen at 5.6 T at 260 GHz in Figure 4 and at 10.35 T at 406.4 GHz in Figure S5. The line widths of the other transitions were generally smaller but followed the same trend.

transition: $|S, M_S\rangle = |2, -1\rangle \rightarrow |2, 0\rangle$ as observed at 10 K and 203 GHz in Figure 2. Similar trends were observed at other frequencies, and although the absolute values differ between particular $|S, M_S\rangle$ transitions and perpendicular/parallel turning points, the line width increase with the increase of Mn(III) content was always observed. The line width also increased for the same x, at a fixed temperature, and for the same turning point, while increasing frequency/field, which is a common phenomenon in EPR and particularly HFEPR, usually attributed to g-strain.

There are several conclusions that can be drawn from the above results. First, and most elementary, the EPR results confirm the observation of suppressing the paramagnetic/antiferromagnetic transition in the $YIn_{1-x}Mn_xO_3$ solid solutions for any $x < 0.5$ since the spectra such as shown in Figures 2 and 4 clearly correspond to those of a paramagnetic spin system, not an antiferromagnetic one.

Second, the spin Hamiltonian parameters obtained from the spectra fall into the range previously observed for HS ($S = 2$) Mn(III) in a variety of coordination complexes.[34] In particular, the zfs parameter D is known to vary from ca. −4.5 cm^{-1} in quasi-octahedral complexes with a Jahn−Teller elongation to ca. +3 cm^{-1} in those with a Jahn−Teller compression. The square-pyramidal Mn(III) complexes such as those found in porphyrinoid complexes typically display D in the range from −3 cm^{-1} to −1.5 cm^{-1}. The current result, yielding D of +3 cm^{-1}, adds to our knowledge of the electronic properties of Mn(III). Whether this value is characteristic for Mn(III) in TBP coordination will only be proven when more systems with the same coordination are studied. We note that the distorted TBP Mn(III) complex studied by Gupta et al.[25] gave D = +1.7(5) cm^{-1} (with a small rhombic splitting, $E/D = 0.05$). A biological five-coordinate Mn(III) center (in manganese superoxide dismutase (MnSOD) also exhibited $D > 0$ (D = +2.10 cm^{-1}, $E/D = 0.11$).[28] Qualitatively, the positive sign of D follows the observations in distorted octahedral complexes, where, as shown by ligand-field theory (LFT),[15,24] $D > 0$ is

DOI: 10.1021/acs.inorgchem.5b01306
Inorg. Chem. 2015, 54, 9040−9045

characteristic for a tetragonal compression of the octahedron[17,20,35] (hole in d_{z^2}), yielding a $^5A_{1g}$ (in D_{4h}) ground state. For such six-coordinate complexes, a tetragonal elongation, the more common scenario, gives $D < 0$ arising from a $^5B_{1g}$ ground state (hole in $d_{x^2-y^2}$).[15] For TBP coordination, an extreme case of axial elongation would give a $^5E'$ (hole in d_{xy},$d_{x^2-y^2}$) ground state. In this case, there would be first-order spin−orbit coupling (SOC) leading to large zfs that could not be well-described by an $S = 2$ spin Hamiltonian,[36] clearly not the case here. In the current series the apical Mn−O bond lengths are markedly smaller than that of the three equatorial Mn−O bonds, structurally corresponding to a trigonal compression of the ideal bipyramid.

The zfs in a $[MnO_5]$ coordination sphere can be further probed quantitatively using a simple ligand-field model. Very sophisticated crystal-field models have been used to analyze optical spectra of Mn^{3+} and Mn^{4+} ions in zirconia (i.e., O6 donor set),[37] but these are beyond our primarily EPR study. Likewise, advanced quantum chemical methods have been applied to Mn(III) in molecular complexes,[35,38] including polynuclear systems,[39] but as shown in the following, a relatively simple semiquantitative LFT approach yields very satisfactory results in this particular case. For a single electron/hole system, such as the case here, considering only σ-bonding, use of the angular overlap model (AOM) for ideal TBP geometry gives the $^5E'$ excited state at an energy of $(13/8)\varepsilon_\sigma$ above the $^5A_1'$ ground state and the $^5E''$ excited state (hole in d_{xz},d_{yz}) at $(11/4)\varepsilon_\sigma$.[3,40] Use of the experimental energy for the $^5A_1' \rightarrow {}^5E'$ transition of 2 eV thus gives $\varepsilon_\sigma \approx 9900$ cm^{-1}. We then perform a calculation with the program Ligfield[41] using the entire d^4 basis set with B and C (Racah electron−electron repulsion) and ζ (single electron SOC constant) parameters set at 85% of their free-ion values,[42−44] respectively, 810 cm^{-1}, 3500 cm^{-1}, and 300 cm^{-1}. This calculation gives the $^5E'$ excited state at 15 820−16 420 cm^{-1} above the ground state, in good agreement with experiment, and $D_{SOC} = +2.06$ cm^{-1}.[45] Although this calculated value for zfs is too low, importantly, it has the correct sign. The effect of axial compression can also be considered using the AOM. In this case, the $^5E'$ excited state is at an energy of $2\varepsilon_{\sigma_{ax}} - (3/8)\varepsilon_{\sigma_{eq}}$, and the $^5E''$ excited state is at $2\varepsilon_{\sigma_{ax}} + (3/4)\varepsilon_{\sigma_{eq}}$. How can these two bonding directions be distinguished? The difference in bond lengths between axial and equatorial Mn−O bonds can be parametrized by an r^{-5} relationship,[46] which we have also used previously.[47] In the present case: $(\varepsilon_{\sigma(Mn-O_{ax})})/(\varepsilon_{\sigma(Mn-O_{eq})}) = (r^5_{(Mn-O_{eq})})/(r^5_{(Mn-O_{ax})})$, where $r_{(Mn-O_{eq})avg} = 2.0553$ Å and $r_{(Mn-O_{ax})_{avg}} = 1.8645$ Å,[48,49] so that $\varepsilon_{\sigma(Mn-O_{ax})} = 1.6277(\varepsilon_{\sigma(Mn-O_{eq})})$. Substituting this relation into the above equation for the $^5E'$ excited state energy gives $\varepsilon_{\sigma_{ax}} = 9115$ cm^{-1} and $\varepsilon_{\sigma_{eq}} = 5600$ cm^{-1}, likely overstating the effect, but still instructive.[50] A calculation using otherwise the same parameters as above then gives $D = +2.44$ cm^{-1}.[51] This value is slightly lower than that obtained by experiment, but a mitigating factor is that the contribution to zfs from spin−spin coupling (SSC) is not included. In his pioneering study of zfs in $Mn(acac)_3$, a system that resembles ours, Neese showed that $D_{SSC} \approx (1/3)D_{SOC}$.[38] The effect of SSC was further elaborated on by Duboc et al.[52] Thus, the total $D = D_{SOC} + D_{SSC}$ could be estimated as ca. +3 cm^{-1}, essentially the same as experiment.

We also note that in $YInO_3$,[53] where there is no operative Jahn−Teller effect, there is still a slight axial compression: $r_{(In-O_{eq})avg} = 2.1133$ Å and $r_{(In-O_{ax})_{avg}} = 2.0875$, so that $\varepsilon_{\sigma(In-O_{ax})} = 1.0633(\varepsilon_{\sigma(In-O_{eq})})$, which gives $\varepsilon_{\sigma_{ax}} = 9770$ cm^{-1} and $\varepsilon_{\sigma_{eq}} = 9190$ cm^{-1}. This represents the extreme of the structure being constrained to that of the diamagnetic host lattice. An analogous calculation then gives $D_{SOC} = +2.13$ cm^{-1}, also close to experiment when the above estimated D_{SSC} is included.

For completeness, we note that it could be possible to include axial and equatorial π-bonding in our AOM. In this case, the $^5E'$ excited state is at an energy of $2\varepsilon_{\sigma_{ax}} - (3/8)\varepsilon_{\sigma_{eq}} + 2\varepsilon_{\pi_{ax}} + (3/2)\varepsilon_{\pi_{eq}}$, and the $^5E''$ excited state is again at higher energy, assuming that $\varepsilon_\sigma > |\varepsilon_\pi|$, $2\varepsilon_{\sigma_{ax}} + (3/4)\varepsilon_{\sigma_{eq}} + (3/2)\varepsilon_{\pi_{eq}}$. With only one experimental d−d transition and no clear way of distinguishing axial versus equatorial π-bonding, it is not worthwhile to attempt to quantify this effect. We simply note that the oxide ions would likely be π-donors, so their σ-bonding parameters obtained from only σ-bonding would be reduced.

Third, concerning the appearance of the HFEPR spectra, the broadening of the EPR resonances with increasing Mn(III) content as seen in Figure 2 is easy to understand qualitatively: the increased Mn(III) concentration leads to reducing an average Mn−Mn distance, and thus increased spin−spin interactions, which are a primary cause of this effect. The HFEPR spectra of $YIn_{1-x}Mn_xO_3$ solid solutions are unusual in that they can be observed from liquid helium to room temperatures. The particular temperature behavior of the spectra depends on the Mn(III) concentration factor x: while for $x < 0.2$ the intensity of the spectra follows Curie behavior with no significant change in the line widths (Figure S6), for the most concentrated solutions ($x = 0.5$) an increase in temperature brings about a new, very broad ($\Delta B_{pp} \approx 0.7$ T at 150 K) resonance centered on $g = 2.00$ (Figure 5). At high

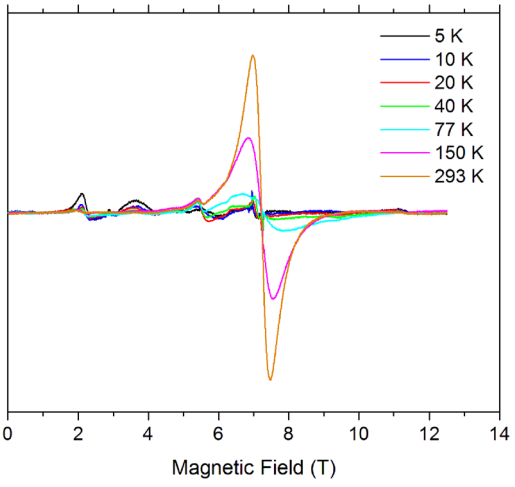

Figure 5. HFEPR spectra of $YIn_{0.5}Mn_{0.5}O_3$ recorded at 203.2 GHz and varying temperatures, as indicated in the figure, obtained with magnetic modulation.

temperatures ($150 < T < 293$ K) this resonance in turn undergoes a narrowing, with the room-temperature line width of ~0.5 T. The origin of the high-temperature resonance can be understood in terms of averaging the zfs through thermally activated spin−spin exchange among the Mn(III) ions, although the thermal activation of this process is not yet understood.

DOI: 10.1021/acs.inorgchem.5b01306
Inorg. Chem. 2015, 54, 9040−9045

In conclusion, the $YIn_{1-x}Mn_xO_3$ material not only exhibits remarkable optical properties, provided the doping level (x) is low, but is also successfully examined by HFEPR. The ultimate goal is to understand and explain the magnetic properties of all of these and similar oxide pigments in the context of their unusual coordination and optical properties. Concerning the use of EPR for such materials, conventional wisdom has it that integer spin systems are "EPR-silent" (i.e., at conventional frequencies and magnetic fields), although this has been long disproven for rhombic $S = 2$ systems.[26−29] Conventional wisdom also has it that integer spin systems (even when examined by HFEPR and are thus no longer "silent", such as the case here) require low temperatures (typically <77 K), yet $YIn_{1-x}Mn_xO_3$ can be easily observed at room temperature, at least for low x. A final tenet of conventional wisdom, albeit only among *aficionados/as* of HFEPR, is that $S = 2$ systems with positive D values are difficult to observe, providing no[54] or at best low-quality spectra (and only in the case of large rhombicity).[17,20,35] Yet $YIn_{1-x}Mn_xO_3$ has $D > 0$, is rigorously axial, and gives high-quality HFEPR spectra, over a wide range of experimental conditions. We suspect that such doped materials, that is, solid solutions, are ideal for HFEPR investigation, regardless of zfs configuration. Moreover, HFEPR complements optical and other experimental methods as being a sensitive probe of dopant level. Oxide and other materials containing HS dopants were studied by early forms of HFEPR,[24] and we suggest that with current instrumentation and software such studies could be very rewarding to the solid-state chemistry/materials science community.

■ ASSOCIATED CONTENT

Supporting Information

The Supporting Information is available free of charge on the ACS Publications website at DOI: 10.1021/acs.inorgchem.5b01306.

Figures showing a diagram of energy levels for the $S = 2$ system with positive axial zfs; field/frequency maps for $YIn_{1-x}Mn_xO_3$, $x = 0.1$ and 0.2; HFEPR spectra of $YIn_{0.9}Mn_{0.1}O_3$ at 109 and 406 GHz; temperature dependent HFEPR spectra at 203 GHz for $x = 0.05$; table of Ligfield output. (PDF)

■ AUTHOR INFORMATION

Corresponding Authors

*Phone: 850 644 6077. E-mail: krzystek@magnet.fsu.edu. (J.K.)

*Phone: 541 737 8235. E-mail: Mas.Subramanian@oregonstate.edu. (M.A.S.)

Author Contributions

The manuscript was written through contributions of all authors. All authors have given approval to the final version of the manuscript.

Funding

The NHMFL is supported by NSF (Cooperative Agreement DMR 1157490), the State of Florida, and the U.S. Department of Energy. The work at Oregon State Univ. was supported by NSF (DMR 0804167; DMR 1216479)

Notes

The authors declare no competing financial interest.

■ ACKNOWLEDGMENTS

We thank Prof. J. Bendix, Copenhagen Univ., for the program Ligfield and Dr. A. Ozarowski, NHMFL, for the EPR simulation and fitting software SPIN and for helpful discussions.

■ REFERENCES

(1) Smith, A. E.; Mizoguchi, H.; Delaney, K.; Spaldin, N. A.; Sleight, A. W.; Subramanian, M. A. *J. Am. Chem. Soc.* **2009**, *131*, 17084−17086.

(2) Mizoguchi, H.; Sleight, A. W.; Subramanian, M. A. *Inorg. Chem.* **2011**, *50*, 10−12.

(3) Miessler, G. L.; Fischer, P. J.; Tarr, D. A. *Inorganic Chemistry;* Pearson: Upper Saddle River, NJ, 2014, pp 382−387.

(4) Dixit, A.; Smith, A. E.; Subramanian, M. A.; Lawes, G. *Solid State Commun.* **2010**, *150*, 746−750.

(5) Smolenskii, G. A.; Bokov, V. A. *J. Appl. Phys.* **1964**, *35*, 915−918.

(6) Telser, J.; Krzystek, J.; Ozarowski, A. *JBIC, J. Biol. Inorg. Chem.* **2014**, *19*, 297−318.

(7) Goldberg, D. P.; Telser, J.; Krzystek, J.; Montalban, A. G.; Brunel, L.-C.; Barrett, A. G. M.; Hoffman, B. M. *J. Am. Chem. Soc.* **1997**, *119*, 8722−8723.

(8) Krzystek, J.; Telser, J.; Pardi, L. A.; Goldberg, D. P.; Hoffman, B. M.; Brunel, L.-C. *Inorg. Chem.* **1999**, *38*, 6121−6129.

(9) Krzystek, J.; Telser, J.; Hoffman, B. M.; Brunel, L.-C.; Licoccia, S. *J. Am. Chem. Soc.* **2001**, *123*, 7890−7897.

(10) Harvey, J. D.; Ziegler, C. J.; Telser, J.; Ozarowski, A.; Krzystek, J. *Inorg. Chem.* **2005**, *44*, 4451−4453.

(11) Barra, A.-L.; Gatteschi, D.; Sessoli, R.; Abbati, G. L.; Cornia, A.; Fabretti, A. C.; Uytterhoeven, M. G. *Angew. Chem., Int. Ed. Engl.* **1997**, *36*, 2329−2331.

(12) Limburg, J.; Vrettos, J. S.; Crabtree, R. H.; Brudvig, G. W.; de Paula, J. C.; Hassan, A.; Barra, A.-L.; Duboc-Toia, C.; Collomb, M.-N. *Inorg. Chem.* **2001**, *40*, 1698−1703.

(13) Mossin, S.; Weihe, H.; Barra, A.-L. *J. Am. Chem. Soc.* **2002**, *124*, 8764−8765.

(14) Krzystek, J.; Telser, J. *J. Magn. Reson.* **2003**, *162*, 454−465.

(15) Krzystek, J.; Yeagle, G.; Park, J.-H.; Meisel, M. W.; Britt, R. D.; Brunel, L.-C.; Telser, J. *Inorg. Chem.* **2003**, *42*, 4610−4618.

(16) Krzystek, J.; Yeagle, G. J.; Park, J.-H.; Britt, R. D.; Meisel, M. W.; Brunel, L.-C.; Telser, J. *Inorg. Chem.* **2009**, *48*, 3290−3290.

(17) Mantel, C.; Hassan, A. K.; Pécaut, J.; Deronzier, A.; Collomb, M.-N.; Duboc-Toia, C. *J. Am. Chem. Soc.* **2003**, *125*, 12337−12344.

(18) Aromí, G.; Telser, J.; Ozarowski, A.; Brunel, L.-C.; Stoeckli-Evans, H.-M.; Krzystek, J. *Inorg. Chem.* **2005**, *44*, 187−196.

(19) Krivokapic, I.; Noble, C.; Klitgaard, S.; Tregenna-Piggott, P. L. W.; Weihe, H.; Barra, A.-L. *Angew. Chem., Int. Ed.* **2005**, *44*, 3613−3616.

(20) Scheifele, Q.; Riplinger, C.; Neese, F.; Weihe, H.; Barra, A.-L.; Juranyi, F.; Podlesnyak, A.; Tregenna-Piggott, P. L. W. *Inorg. Chem.* **2008**, *47*, 439−447.

(21) Sunatsuki, Y.; Kishima, Y.; Kobayashi, T.; Yamaguchi, T.; Suzuki, T.; Kojima, M.; Krzystek, J.; Sundberg, M. R. *Chem. Commun.* **2011**, *47*, 9149−9151.

(22) Forshaw, A. P.; Smith, J. M.; Ozarowski, A.; Krzystek, J.; Smirnov, D.; Zvyagin, S. A.; Harris, T. D.; Karunadasa, H. I.; Zadrozny, J. M.; Schnegg, A.; Holldack, K.; Jackson, T. A.; Alamiri, A.; Barnes, D. M.; Telser, J. *Inorg. Chem.* **2013**, *52*, 144−159.

(23) Vallejo, J.; Pascual-Álvarez, A.; Cano, J.; Castro, I.; Julve, M.; Lloret, F.; Krzystek, J.; De Munno, G.; Armentano, D.; Wernsdorfer, W.; Ruiz-García, R.; Pardo, E. *Angew. Chem., Int. Ed.* **2013**, *52*, 14075−14079.

(24) Gerritsen, H. J.; Sabisky, E. S. *Phys. Rev.* **1963**, *132*, 1507−1512.

(25) Gupta, R.; Taguchi, T.; Borovik, A. S.; Hendrich, M. P. *Inorg. Chem.* **2013**, *52*, 12568−12575.

(26) Münck, E.; Surerus, K. K.; Hendrich, M. P. *Methods Enzymol.* **1993**, *227*, 463−479.

(27) Hendrich, M. P.; Debrunner, P. G. *Biophys. J.* **1989**, *56*, 489−506.

DOI: 10.1021/acs.inorgchem.5b01306
Inorg. Chem. 2015, 54, 9040−9045

(28) Campbell, K. A.; Yikilmaz, E.; Grant, C. V.; Gregor, W.; Miller, A.-F.; Britt, R. D. *J. Am. Chem. Soc.* **1999**, *121*, 4714−4715.
(29) Campbell, K. A.; Lashley, M. R.; Wyatt, J. K.; Nantz, M. H.; Britt, R. D. *J. Am. Chem. Soc.* **2001**, *123*, 5710−5719.
(30) Hassan, A. K.; Pardi, L. A.; Krzystek, J.; Sienkiewicz, A.; Goy, P.; Rohrer, M.; Brunel, L.-C. *J. Magn. Reson.* **2000**, *142*, 300−312.
(31) Zvyagin, S. A.; Krzystek, J.; van Loosdrecht, P. H. M.; Dhalenne, G.; Revcolevschi, A. *Phys. B* **2004**, *346*−*347*, 1−5.
(32) Because of the linewidth, no hyperfine coupling to ^{55}Mn (I = 5/2, 100%) is resolved, even for lower values of x. Such hyperfine coupling has been resolved for $[Mn(H_2O)_6]^{3+}$ as a dopant in cesium gallium alum,[19] but this required a single-crystal study.
(33) Krzystek, J.; Zvyagin, S. A.; Ozarowski, A.; Trofimenko, S.; Telser, J. *J. Magn. Reson.* **2006**, *178*, 174−183.
(34) Telser, J.; Ozarowski, A.; Krzystek, J. In *Electron Paramagnetic Resonance;* The Royal Society of Chemistry: London, U.K., 2013; Vol. *23*, pp 209−263.
(35) Cazacu, M.; Shova, S.; Soroceanu, A.; Machata, P.; Bucinsky, L.; Breza, M.; Rapta, P.; Telser, J.; Krzystek, J.; Arion, V. B. *Inorg. Chem.* **2015**, *54*, 5691−5706.
(36) McGarvey, B. R.; Telser, J. *Inorg. Chem.* **2012**, *51*, 6000−6010.
(37) Klokishner, S. I.; Reu, O.; Chan-Thaw, C. E.; Jentoft, F. C.; Schlögl, R. *J. Phys. Chem. A* **2011**, *115*, 8100−8112.
(38) Neese, F. *J. Am. Chem. Soc.* **2006**, *128*, 10213−10222.
(39) Retegan, M.; Cox, N.; Pantazis, D. A.; Neese, F. *Inorg. Chem.* **2014**, *53*, 11785−11793.
(40) Schäffer, C. E. *Struct. Bonding (Berlin)* **1968**, *5*, 68−95.
(41) Bendix, J. In *Comprehensive Coordination Chemistry II, Vol. 2: Fundamentals: Physical Methods, Theoretical Analysis, and Case Studies;* Lever, A. B. P., Ed.; Elsevier: Amsterdam, The Netherlands, 2003; Vol. *2*, pp 673−676.
(42) Bendix, J.; Brorson, M.; Schäffer, C. E. *Inorg. Chem.* **1993**, *32*, 2838−2849.
(43) Brorson, M.; Schäffer, C. E. *Inorg. Chem.* **1988**, *27*, 2522−2530.
(44) A reduction of 71% was used for Mn^{3+} in rutile,[24] that is, six oxide nearest neighbors rather than five; 0.85 = 0.71(6/5).
(45) If the calculation uses only the quintet states of Mn(III) (i.e., only those derived from ^{5}D free ion), then D_{SOC} = +0.77 cm^{-1}, demonstrating the importance of contributions from the triplet excited states to zfs.
(46) Larrabee, J. A.; Johnson, W. R.; Volwiler, A. S. *Inorg. Chem.* **2009**, *48*, 8822−8829.
(47) Krzystek, J.; Ozarowski, A.; Zvyagin, S. A.; Telser, J. *Inorg. Chem.* **2012**, *51*, 4954−4964.
(48) Yakel, H. L., Jr.; Koehler, W. C.; Bertaut, E. F.; Forrat, E. F. *Acta Crystallogr.* **1963**, *16*, 957−962.
(49) van Aken, B. B.; Meetsma, A.; Palstra, T. T. M. *Acta Crystallogr., Sect. C: Cryst. Struct. Commun.* **2001**, *57*, 230−232.
(50) Slightly different rounding could give these as $\varepsilon_{\sigma_{ax}}$ = 9100 cm^{-1} and $\varepsilon_{\sigma_{eq}}$ = 5590 cm^{-1}, thus giving a range of values using this model.
(51) This calculation gives the ^{5}E′ excited state at 15 930−16 480 cm^{-1}, in agreement with experiment, and the ^{5}E″ excited state at 22 270−22 600 cm^{-1}.
(52) Duboc, C.; Ganyushin, D.; Sivalingam, K.; Collomb, M.-N.; Neese, F. *J. Phys. Chem. A* **2010**, *114*, 10750−10758.
(53) Pistorius, C. W. F. T.; Kruger, G. J. *J. Inorg. Nucl. Chem.* **1976**, *38*, 1471−1475.
(54) Romain, S.; Duboc, C.; Neese, F.; Rivière, E.; Hanton, L. R.; Blackman, A. G.; Philouze, C.; Leprêtre, J.-C.; Deronzier, A.; Collomb, M.-N. *Chem. - Eur. J.* **2009**, *15*, 980−988.

DOI: 10.1021/acs.inorgchem.5b01306
Inorg. Chem. 2015, 54, 9040−9045